Environmental Science
Processes & Impacts

Urban soil exploration through multi-receiver electromagnetic induction and stepped-frequency ground penetrating radar

Journal:	*Environmental Science: Processes & Impacts*
Manuscript ID:	EM-ART-01-2015-000023.R1
Article Type:	Paper
Date Submitted by the Author:	11-Apr-2015
Complete List of Authors:	Van De Vijver, Ellen; Ghent University, Soil Management Van Meirvenne, Marc; Ghent University, Soil Management Vandenhaute, Laura; Ghent University, Soil Management Delefortrie, Samuël; Ghent University, Soil Management De Smedt, Philippe; Ghent University, Soil Management Saey, Timothy; Ghent University, Soil Management Seuntjens, Piet; Ghent University, Soil Management; Flemish Institute for Technological Research (VITO),

Environmental impact statement

The proper management of urban soils is a key issue in our urbanizing world. However, the heterogeneity of these soils poses severe challenges to the conventional soil survey approach that relies on spatially discrete observations from soil borings and groundwater monitoring wells. Non-invasive geophysical techniques provide a cost-effective alternative to investigate soil in a spatially comprehensive way. This study demonstrates the high-resolution application of multi-receiver electromagnetic induction and stepped-frequency ground penetrating radar on a contaminated former garage site. Various geophysical anomalies that can serve as a proxy for different anthropogenic soil disturbances are indicated. These results highlight how these sensing technologies can contribute to urban soil assessment and management.

Urban soil exploration through multi-receiver electromagnetic induction and stepped-frequency ground penetrating radar

Ellen Van De Vijver[a*], Marc Van Meirvenne[a], Laura Vandenhaute[a], Samuël Delefortrie[a], Philippe De Smedt[a], Timothy Saey[a] and Piet Seuntjens[a,b,c]

[a]Department of Soil Management, Ghent University, Coupure links 653, 9000 Gent, Belgium

[b]Flemish Institute for Technological Research (VITO), Land and Water Management, Boeretang 200, 2400 Mol, Belgium

[c]Department of Bio-engineering Sciences, University of Antwerp, Groenenborgerlaan 171, 2020 Antwerpen, Belgium

*Corresponding author:

e-mail: ervdevij.vandevijver@UGent.be, tel.: +32 (0) 9 264 58 69, fax: +32 (0) 9 264 62 47

Abstract

In environmental assessments, the characterization of urban soils relies heavily on invasive investigation, which is often insufficient to capture their full spatial heterogeneity. Non-invasive geophysical techniques enable rapid collection of high-resolution data and provide a cost-effective alternative to investigate soil in a spatially comprehensive way. This paper presents the results of combining multi-receiver electromagnetic induction and stepped-frequency ground penetrating radar to characterize a former garage site contaminated with petroleum hydrocarbons. The sensor combination showed the ability to identify and accurately locate building remains and a high-density soil layer, thus demonstrating the high potential to investigate anthropogenic disturbances of physical nature. In addition, a correspondence was found between an area of lower electrical conductivity and elevated concentrations of petroleum hydrocarbons, suggesting the potential to detect specific chemical disturbances. We conclude that the sensor combination provides valuable information for preliminary assessment of urban soils.

Key words

Urban soils, geophysical techniques, electromagnetic induction, ground penetrating radar, soil contamination, petroleum hydrocarbons

1 Introduction

In a world with accelerating urbanization, urban soil management is of continuously growing importance (*e.g.* De Kimpe and Morel,[1] Lehmann and Stahr[2]). Meuser[3] defines 'urban soils' as "soils in urban and suburban areas consisting of anthropogenic deposits with natural (mineral, organic) and technogenic materials, formed and modified by cutting, filling, mixing, intrusion of liquids and gases, sealing and contamination". This definition argues one of the most important motives behind urban soil investigation as well as the challenges involved in doing this. As urban soils may be contaminated, they often become the subject of environmental assessments setting out the management strategy towards the future land use destination.[4] Whereas identifying soil contamination can be considered the main aim of contaminated site assessment, characterizing the host soil matrix also is critical to understanding contaminant migration and distribution.[5] Conventional soil investigation, commonly including soil coring, soil sampling and well monitoring, is expensive and usually only provides information from a limited number of observation points. Furthermore, these are small localized measurements of which the location can be biased depending on the a priori available site information and the expertise of the professionals involved. Therefore, the typically large spatial heterogeneity of urban soils can affect the reliability and representativeness of conventional soil survey results.

Non-invasive geophysical techniques allow rapid collection of high-resolution data, enabling to narrow the spatial information gaps between invasive observations. In this paper, we focus on electromagnetic induction (EMI) and ground penetrating radar (GPR). Both techniques have an established reputation for the indirect mapping of spatial variations in 'natural' soil properties such as soil texture, soil moisture and organic matter (OM) content as evidenced by numerous studies in the field of precision agriculture (*e.g.* Adamchuk *et al.*,[6] Corwin and Lesch[7]). The suitability of EMI and GPR for identifying physical artefacts such as building remains, ditches and remoulded or refilled soil material and investigating their surrounding soil context has been demonstrated in a number of recent studies in landscape archaeology (*e.g.* Verdonck *et al.*,[8] De Smedt *et al.*,[9] Saey *et al.*[10]). The detection of petroleum hydrocarbons and their interactions with their host soil environment is an important example of the chemical counterpart of this problem. In the search for a non-invasive solution, several authors have studied the electrical properties (electrical conductivity and dielectric permittivity) of hydrocarbon contaminated soils. Mainly focusing on the application of GPR, these properties have been theoretically estimated, often using laboratory measurements as calibration (*e.g.* Carcione *et al.*,[11] Cassidy[12]), and have been measured under laboratory and controlled field conditions (*e.g.* Brewster *et al.*,[13] Daniels *et al.*,[14] Santamarina and Fam[15]). Fewer studies have been conducted on the use of EMI for detecting hydrocarbon contamination (*e.g.* Jin *et al.*,[16] Martinelli *et al.*[17]). However, recognizing the complexity of this geophysical problem and the advantage of a multi-sensor approach, most uncontrolled field studies have used a combination of EMI and GPR and possibly other techniques (*e.g.* Atekwana *et al.*,[18] Guy *et al.*[19]). Because the concentration and composition of a petroleum hydrocarbon contamination and the bio-physicochemical conditions of its soil environment vary in space and time, the electrical response of hydrocarbon contaminated soils is very complex. Petroleum hydrocarbons commonly have a very low intrinsic conductivity (0.0001 to 0.001 mS/m according to Carcione *et al.*[11]) and thus initially reduce the soil electrical conductivity when displacing water in the pore space. Due to physico-chemical changes of the contaminated environment induced by biodegradation processes, with time the geophysical response generally changes from being less conductive to more conductive. The time required for this change to occur varies and exceptions have been reported (*e.g.* de la Vega[20]), but the usual behaviour is that hydrocarbon contaminated soil volumes eventually present anomalously high conductivity.[5, 21-23] In any case urban soils provide interesting environments to explore the combination of EMI and GPR as they encompass various soil variations of natural and anthropogenic origins. However, the application of both EMI and GPR to address the integral problem of urban soil investigation remains poorly studied.

Following the trend towards denser 3D surveying (Auken *et al.*[24]), we have used a motorized setup of a multi-receiver EMI sensor and a stepped-frequency GPR system operating with an antenna array. Our objective was to investigate the potential contribution of these state-of-the-art soil sensors to urban soil investigation, including detection and identification of physical and chemical anomalies.

2 Materials and methods

2.1 Study site

The study site is located in an urban area of West-Flanders, Belgium. It consists of a former garage with petrol station and storage of accident-involved vehicles (Fig. 1) that was active from 1976 to 2012. An environmental assessment was carried out between 2008 and 2012, in which soil information was collected from borings and groundwater monitoring wells at the locations indicated in Fig. 1. These locations were clustered around the location of two underground storage tanks for diesel and gasoline, while large other parts of the study site were only sparsely covered. Based on the soil borings, soil texture was described as sandy for the first two meters below the surface and as loamy sandy between two and three meter. The groundwater table was situated at a depth between 2 and 2.5 m. Based on the laboratory analyses of soil and groundwater samples, a contamination with petroleum hydrocarbons and BTEX was found. Fig. 1 shows the spatial extent of the soil contamination with petroleum hydrocarbons as defined by testing the total petroleum hydrocarbon (TPH, C10-C40) concentration against the thresholds provided by the Flemish soil remediation legislation (VLAREBO).[25]

To obtain useful soil data from EMI and GPR, the survey area has to be exempt, as much as possible, of surface or aboveground metallic structures. Therefore, our survey area was limited to a 1050 m² part of the car parking area covered with limestone gravel, where the vehicles had already been removed (Fig. 1).

Fig. 1 near here

2.2 EMI survey

The apparent electrical conductivity (EC_a) of the soil was surveyed using a frequency-domain EMI sensor. We refer to Keller and Frischknecht[26] for a detailed theoretical description of the application of EMI techniques to measuring soil EC_a; McNeill[27] gives a more practical summary for operation under conditions of low induction number, which were adopted here. In this study, a DUALEM-21S sensor (DUALEM Inc., Milton, Canada) was used. This multi-receiver EMI sensor has an operating frequency of 9 kHz and contains four coil configurations: one transmitter coil paired with four receiver coils at spacings of 1 m, 1.1 m, 2 m and 2.1 m. The 1 m and 2 m transmitter-receiver pairs have a horizontal coplanar orientation (1HCP and 2HCP), while the 1.1 m and 2.1 m pairs have a perpendicular orientation (1PRP and 2PRP). Due to a different transmitter-receiver spacing and orientation, the four coil configurations have a different depth sensitivity for measuring the soil EC_a.[26, 27] To link the four EC_a responses to the respective soil volumes they represent, the depth of exploration (DOE) has been conventionally defined as the depth where 70% of the cumulative response is obtained from the soil volume above this depth. For the 1PRP, 2PRP, 1HCP and 2HCP coil configurations the DOE is 0.5 m, 1.0 m, 1.6 m and 3.2 m, respectively.[28] The multi-receiver EMI sensor thus provides simultaneous EC_a measurements representative of these four different soil volumes.

The EMI sensor was mounted in a sled pulled by an all-terrain vehicle (ATV). A Leica Viva GNSS-G15 differential GPS (Leica Geosystems, Heerbrugg, Switserland) was used to georeference the measurements with a pass-to-pass accuracy of less than 0.1 m. The area was surveyed along parallel lines 0.9 m apart and, with a sampling rate of 8 Hz and a driving speed around 8 km/h, the in-line distance between two measurements was circa 0.25 m. Afterwards, the measurement coordinates were corrected for the spatial offset between the GPS antenna and the centre of the transmitter-receiver coil pairs of the EMI sensor.[29] The measured EC_a values were standardized to a reference temperature of 25 °C using the formula presented in Sheets and Hendrickx.[30] To map the EC_a data, they were interpolated to a grid with 0.1 m cell size using ordinary point kriging.[31]

Additionally, the four EC_a measurements were combined into the 'fused electromagnetic metal prediction' (FEMP) as developed by Saey *et al.*[32] to investigate the presence of subsurface metallic structures. To remove the influence from background EC_a variations and to focus on local anomalies, the EC_a measurements were 'detrended' by subtracting the moving average within a circular window with a radius of 4 m. The FEMP was then calculated as the following linear combination of the residual EC_a values:[32]

$$\mathrm{FEMP} = 2.05 \cdot \Delta \mathrm{EC}_{\mathrm{a,\,1PRP}} - 1 \cdot \Delta \mathrm{EC}_{\mathrm{a,\,2PRP}} - 0.82 \cdot \Delta \mathrm{EC}_{\mathrm{a,\,1HCP}} - 1.89 \cdot \Delta \mathrm{EC}_{\mathrm{a,\,2HCP}}$$

which provides a measure for the probability of the occurrence of a metallic object.

2.3 GPR survey

In this study, GPR data were collected using a stepped-frequency continuous wave (SFCW) system (GeoScope-GS3F, 3d-Radar AS, Trondheim, Norway). This system produces a waveform consisting of a sequence of sine waves with linearly increasing frequencies within the range of 100 to 3000 MHz. While a conventional impulse GPR requires a centre frequency to be chosen beforehand, as a trade-off between the desired penetration depth and vertical resolution, the wide frequency bandwidth adopted by a SFCW system offers an optimal resolution for each achievable penetration depth. Furthermore, a SFCW system focuses energy in one single frequency at a time and the phase and amplitude of the reflected signal is recorded for each discrete frequency step which anticipates an improved penetration depth and signal-to-noise ratio (SNR).[33] As the data are recorded in frequency domain, an inverse Fourier transform needs to be applied to visualize the data in time-domain profiles. The SFCW system operates with an array of multiple fixed-offset antenna pairs that can collect data quasi-simultaneously, expediting full spatial coverage of the survey area. Here, a V1213 antenna array was used including 13 antenna-receiver combinations at a uniform spacing of 0.075 m, providing a total scan width of 0.975 m.

Similar to the EMI survey, the GPR system was used in a motorized configuration with real-time georeferencing (Trimble AgGPS 332 GPS receiver with OmniSTAR correction, Trimble Navigation Ltd., Sunnyvale, California). The antenna array was mounted on a trailer, with the GPS antenna on top of its centre. To achieve full-area coverage, the driving pattern ensured a minimal overlap of 0.1 m between two adjacent scans. The inline distance between two measurements was fixed at 0.05 m and was controlled by an odometer integrated within one of the trailer wheels. The acquisition frequency range of the SFCW system was adjusted to 100-1500 MHz and was stepped in intervals of 2 MHz with a 2 μs duration of each frequency step.

Post-acquisition data processing started with an interference suppression in frequency domain: for each measurement location, the frequency spectrum of the received signal is analyzed and frequencies with outlying power are suppressed. Afterward, the data are converted to time domain through an inverse fast Fourier transform. A Kaiser window with a beta value of 6 was applied, while the recorded frequency bandwidth was narrowed to 150-800 MHz to reduce both low- and high-frequency noise. Time zero was estimated as the average two-way travel time where the highest magnitude occurred, and was assumed identical over the survey area. Through a horizontal high-pass filter, 90% of the background was removed, 10% was preserved to avoid the complete removal of possible reflections from horizontal soil contrasts. An additional horizontal filter of which the filter size increased with depth further improved the SNR. Prior to visualization, the originally overlapping scans with horizontal measurement resolution of 7.5 cm by 5 cm were subsampled to a 10 cm square grid using a nearest-neighbour interpolation in which priority increased according to the 'centrality' of the transmitter-receiver pair in the antenna array. This procedure thus suppressed the sampling of GPR traces from outer antenna pairs as they are generally more susceptible to interference. Finally, for the trace subsample, the median magnitude was equalized in depth using automatic gain control (AGC).[34] The resulting 3D data volume was then visualized in a selection of relevant vertical and horizontal slices.

2.4 Soil borings and sample analysis

Because of the scarce soil borings in the survey area, the survey results caused us to select an additional number of locations (areas of 1 m by 1 m) for boring investigation. Depending on the observed EC_a and/or GPR contrast and the local field conditions, different means of invasive investigation were deployed.

2.4.1 Soil profile description

After removing the gravel cover with a spade, a gouge auger was used to investigate the soil profile in successive 0.5 m depth intervals. The investigation depth was limited by the groundwater table or by impenetrable material. In the profile description, the soil horizons and their composing materials were identified, with special attention for human-induced soil features (*e.g.* compaction) and technogenic materials (*e.g.* brick fragments, concrete debris).

2.4.2 EC-probe measurements

At each location where the soil profile was described, a second sequence of gouge-auger borings was made to investigate the vertical electrical conductivity variation through EC-probe measurements (14.01 EC-probe, Eijkelkamp Agrisearch Equipment, Giesbeek, The Netherlands). The probe contains four ring-shaped electrodes, spaced 0.025 m apart, that measure the soil resistivity based on the Wenner method.[35] The measured resistivity is representative for an 80 cm^3 elliptic volume around the probe. An additional sensor in the EC-probe's cone recorded the soil temperature. The soil resistivity was then converted to electrical conductivity (EC_p), for a reference temperature of 25 °C. EC_p measurements were made for each 0.1 m depth interval down to the groundwater table.

2.4.3 Soil texture analysis

Using an Edelman hand auger, borings down to 2 m depth were made and for each depth interval of 0.2 m a soil sample was taken. The samples were analyzed following the conventional sieve-pipette method[36] resulting in three textural fractions: clay (0-2 μm), silt (2-50 μm) and sand (50-2000 μm).

2.4.4 TPH concentration analysis

A mixed sample per soil horizon (as identified in the soil profile) was taken for laboratory analysis of the TPH concentration. This analysis was preceded by the spectrophotometric determination of the OM content. The TPH concentration was determined by gas chromatography with flame ionization detector.[37] The limit of detection (LOD) for this procedure is 20 mg/kg dry matter (DM).

3 Results and discussion

3.1 EC_a data

The four EC_a maps are shown in Fig. 2a. The median EC_a is 15.1 mS/m, 20.3 mS/m, 22.4 mS/m and 27.6 mS/m for the 1PRP, 2PRP, 1HCP and 2HCP coil configuration, respectively. As the median EC_a increases with an increasing DOE of the coil configurations, the EC_a generally increases with depth. All four EC_a signals have an extremely high variance due to both negative and positive extreme values; the coefficient of variation (CV) varies between 92% for the 1HCP coil configuration and 201% for the 1PRP coil configuration. The majority of the extreme EC_a values spatially coincide in the four EC_a maps. This is a typical indication for metallic objects (*e.g.* Van De Vijver *et al.*[38]) as is confirmed by the FEMP map (Fig. 2b).[32] A marked group of these 'metal anomalies' is seen in the western corner of the study area (anomaly A, Fig. 2c). The strip of extreme EC_a values at the southeastern edge of the survey area is explained by the metal-reinforced concrete pavement adjoining it. Excluding the extremes, the EC_a measurements are generally in line with the expected values for a sandy to loamy sandy soil (*e.g.* Saey *et al.*[39]). However, in the southern part of the survey area a zone with lower conductivity (anomaly B, Fig. 2c) is observed. This zone consistently appears on all four EC_a maps suggesting correspondence to a soil contrast occurring at a shallow depth, i.e. within about the upper 1 m soil layer.

Fig. 2 near here

3.2 GPR data

Considering the depth at which the AGC gain factor reaches its maximum as an indicator of the depth at which noise becomes dominant, the penetration depth of the GPR signal is approximately 38.3 ns or 1.50 m. The conversion of depth expressed in two-way travel time to depth expressed in meters is based on a time zero of 2.83 ns and a relative dielectric permittivity (RDP) of 12.62. The origin of this RDP value will be explained below. The horizontal variation of the GPR reflection strength is considerably high (CV $\geq$ 65%) within the depth interval from 7.3 ns (or 0.19 m) to 24.9 ns (or 0.93 m), as illustrated in Fig. 3 and Fig. 4. Two features have clearly added to this high signal variation. The first is the high-reflective area in the western corner of the survey area, corresponding to anomaly A defined above. While the spatially exaggerated response of EMI to metallic structures hampered the delineation of this anomaly, the horizontal GPR slices clearly depict its rectangular boundaries (Fig. 3). The vertical profiles allow for a more precise demarcation of the anomaly's vertical extent: for 0 m to 5 m along transect EF strong horizontal reflections are observed starting from the ground surface down to approximately 17 ns (or 0.6 m) depth (Fig. 4). From a depth of about 13 ns (or 0.4 m) downwards on Fig. 3, the horizontal slices display a second notable contrast in reflection strength at the location of anomaly B in the EC_a data. Vertical GPR profiles, such as the one shown in Fig. 4, demonstrate that this contrast is part of a slightly dipping interface, with a larger extent than possibly expected from the horizontal slices. In Fig. 4 the interface appears to extend as far as anomaly A. Yet, the lateral increase in reflection strength correlates with the lower conductivity observed in the EC_a maps: the lower the electrical conductivity, the weaker the GPR signal attenuation and thus the stronger the reflections generated from a given soil contrast. Finally, note that the locations where the EC_a data indicated isolated metallic objects generally not correspond to marked anomalies in the horizontal GPR slices, demonstrating that these metallic objects generally have relatively small dimensions.

Fig. 3 near here

Fig. 4 near here

3.3 Soil borings and sample analysis

An overview of the boring results at the six locations indicated in Fig. 2c, is given in Fig. 5. Beneath the 5 to 10 cm thick gravel cover, the observed soil profiles could roughly be divided into three layers (Fig. 5a). First, a rather heterogeneous, brown to yellowish brown topsoil layer was seen. Particularly at location 1, the topsoil contained clear anthropogenic traces such as small brick fragments and rust patches. At all six locations, the bottom of the topsoil was delimited by an abrupt change to a layer with distinctly higher bulk density and contrasting grey to nearly black colour. In addition to the anthropogenic traces encountered within the topsoil, this layer included tiny coal fragments and a petrochemical smell was perceived at its corresponding depth at locations 1 and 3. At locations 4 and 5 the contrasting layer had an abrupt lower boundary, while at the other locations a gradual change into a fairly homogeneous subsoil with light grey to yellowish brown colour was present. The subsoil suggested a dominant natural origin.

In terms of the EC_p, the six locations also demonstrated a comparable vertical profile (Fig. 5b). The topsoil clearly has a lower conductivity and an average jump of about 7 mS/m is observed near the upper boundary of the contrasting soil layer. Together with the soil profile observations, this links the transition from the topsoil to the contrasting soil layer to the interface observed in the GPR data. Consequently, the transition depths observed from the soil profiles were used to estimate the average RDP of the topsoil, which, together with the earlier estimated time zero, was then used to convert the GPR two-way travel time into depth in meters. Despite the stringent assumption of a constant topsoil RDP, Fig. 5a and b evidence a close correspondence between the estimated depth of the GPR interface and the depth of the contrasting layer as observed in the soil profiles and the EC_p measurements. Despite the similar within-profile EC_p trend, the absolute EC_p measurements differ between the different locations. Whereas locations 1 and 6 show a relative constant topsoil EC_p of about 11 mS/m, at locations 2 to 5 the topsoil EC_p shows an additional dip. Below the topsoil, the between-profile differences are less pronounced.

Soil texture analysis was only performed for locations 1, 4 and 6. With an overall average of 7.6% clay, 30.2% silt and 62.2% sand, the soil texture is classified as light sandy loam (Belgian soil texture triangle), which roughly confirms the data provided by the environmental assessment. As illustrated in Fig. 5c, variations in clay fraction are small both within and between the profiles and do not seem to correlate with the soil layering or the

EC_p measurements. The OM content is generally low, varying between 0.5% DM and 1.7% DM. Particularly locations 2, 3 and 6 demonstrate a slightly higher OM content for the contrasting soil layer (Fig. 5c). The depth-weighted average of the OM content is highest at locations 1 and 6 (1.5 and 1.0% DM), although the difference with locations 3 and 4 (0.98 and 0.91% DM) is very small. Each of the analyzed samples has a TPH concentration far below the soil remediation threshold and target value and only for one sample (location 2, 0.5-0.7 m depth) the background value is exceeded (Fig. 5c). Contrary to locations 2 to 5, the TPH concentration hardly exceeds the LOD at locations 1 and 6. Excepting location 3, the profiles show the highest TPH concentration for the contrasting soil layer.

Fig. 5 near here

3.4 Combined interpretation of the EC_a, GPR and borehole data

Anomaly A was clearly delineated by sharp lateral and vertical contrasts in the GPR data. The significant scatter in the GPR signal in this area suggests the presence of coarse debris such as concrete rubble or bricks (*e.g.* Boudreault *et al.*[40]). The shape and dimensions of the anomaly point to remains of a building or comparable structure. The presence of metal as indicated by the EC_a data further adds to this assumption given that old foundations and demolition debris often contains metallic objects such as reinforcing steel bars. The assumption was confirmed by surface building debris and by two soil borings encountering impenetrable material immediately beneath the gravel cover (Fig. 6). A massive, probably reinforced, concrete structure and a brick layer of approximately 0.5 m thickness were encountered. We note that the location of the brick layer did not show the typical low-conductive signature of this material in the ECa data,[40,41,42] which is likely explained by nearby metallic objects dominating the EMI sensor output. An aerial photograph of the site taken in 1986 relates the northeastern and southeastern edges of anomaly with a former fence (Fig. 6). In November 1985, the site owner filed a request for an expansion of the existing garage. Probably the former building and its surrounding aboveground infrastructure were demolished shortly after the aerial photograph had been taken and the demolition debris used to level the area in preparation to the construction of the parking area. The discrete metallic objects scattered over the site likely relate to the former storage of accident-involved vehicles and garage activities.

Fig. 6 near here

Anomaly B is not clearly delineated by the geophysical data, suggesting that this anomaly originates from a more gradual change of soil properties. In the GPR data, this anomaly appeared as a more reflective part of a shallow contrasting interface occurring over a major part of the survey area. Boring investigation allowed linking this interface with an abrupt transition from the topsoil to a highly disturbed layer with considerably higher bulk density. The EC_p measurements showed that the interface not only corresponded with a contrast in RDP, but also with a change in electrical conductivity. In absence of a significant change in soil texture, the increase in conductivity can likely be attributed to the increased bulk density of the contrasting soil layer, thereby suggesting an effect of soil compaction (*e.g.* André *et al.*,[43] Islam *et al.*[44]). Additionally, the slightly higher OM content may have further contributed to a higher conductivity (*e.g.* Omonode and Vyn,[45] Saey et al.[39]). The many anthropogenic disturbances observed for the contrasting soil layer, including its suggested higher compaction, along with its slightly higher OM content and its wide lateral extent indicated by the GPR profiles argue that its upper limit represents a former living surface. Starting from this idea, the GPR reflections defining the bottom of the debris fill in the western corner of the survey area probably coincide with this surface. This hypothesis is further supported by the aerial photograph taken in 1986 (Fig. 6). In any case, the reorganization of the site after 1986 partly explains the heterogeneous appearance of the current topsoil. Through the EC_a and EC_p measurements, the main explanation for the lateral conductivity variability could be related to a variation of the properties of the current topsoil. While clay and OM content are two key 'natural' factors explaining spatial EC_a variations (*e.g.* Kühn *et al.*,[46] Saey et al.[39]), in this case neither properties showed significant lateral variation. Although the observed subtle variations of these properties have contributed to the resulting sensor measurements, these do not fully explain the observed conductivity contrast. This suggests that the observed lateral contrast may also have predominantly anthropogenic cause. Here, TPH concentration is the only property that showed a distinct difference between the boring locations as the LOD was only clearly exceeded at the locations within the low conductive zone. A decrease in electrical conductivity of the upper vadose zone due to the presence of a hydrocarbon contamination has been reported before (*e.g.* DeRyck *et al.*[47]) and has been suggested to relate to vapor effects.[22] A negative correlation between TPH concentration and electrical conductivity generally relies on the assumption that the effect of biodegradation is negligible. Even so, considering previous research (*e.g.* Daniels *et al.*,[14] Sauck,[20] Carcione *et al.*[11]), it is questionable whether TPH concentrations lower than 50 mg/kg DM (equivalent to a hydrocarbon saturation lower than about 0.0001) are able to cause a conductivity decrease of several millisiemens per meter. In this respect, it is more plausible that the slightly elevated TPH concentration is a proxy for a more complex physico-chemical soil disturbance that could not be fully defined by the limited number of properties that were analyzed on the boring samples. Regarding the within-profile coincidence of the highest TPH concentration and the highest conductivity, we propose two hypotheses. The first assumes that each of the observed hydrocarbon concentrations, irrespective of the depth at which they are observed, corresponds to a relatively fresh and, hence, non-degraded contamination. In this case, the higher OM content and soil bulk density have dominated the GPR and EC_p measurements beneath the topsoil, but may have caused a higher retention of petroleum hydrocarbons in the contrasting soil layer.[48,49] The second hypothesis assumes that the hydrocarbon concentrations observed in the contrasting soil layer relate to an older contamination event than those observed in the topsoil and that, with time, biodegradation processes have added to an increase in electrical conductivity of this layer. Which of the two hypotheses is true cannot be determined with absolute certainty because no direct information on the occurrence of biodegradation was available. Yet, for locations 1, 2, 4 and 5, the composition of the hydrocarbon mixture showed smaller fractions of hydrocarbons in the C10 to C20 range in the contrasting soil layer as compared to the topsoil. Considering that the biodegradable fraction of petroleum hydrocarbons mainly consists in C12-C20 hydrocarbons (*e.g.* Minai-Tehrani *et al.*[50]), this may be an indication in favour of the second hypothesis. The contamination of the contrasting layer possibly even dates from before the site was reorganized at the end of the 1980s and in that case may also have a different lateral extent than the topsoil contamination.

6 Conclusions

Our case study demonstrated the use of combining multi-receiver EMI and stepped-frequency GPR to pinpoint locations of anthropogenic soil disturbances, particularly of those having affected physical soil properties. The identification of a soil layer with considerably higher bulk density exemplified the methodology's potential to improve insight in the upper soil stratification, which in turn could aid the understanding of the local soil-forming processes. Furthermore, the sharp delineation of the building remains illustrated the high accuracy that can be achieved in spatially characterizing structures of technogenic material. Since such physical soil contrasts locally can have a strong influence on the distribution and dispersion of contaminants, they can represent important targets in the investigation of contaminated urban soils. The demonstrated correspondence between a zone of remarkably lower electrical conductivity and slightly elevated TPH concentrations suggests the potential for the sensor combination to detect specific chemical soil disturbances too. However, further investigation should aim at the expansion of the presented methodology to other conditions of contamination with petroleum hydrocarbons, including a wider range of concentrations and biodegradation stages.

This case study proves the advantage of the sensors to rapidly screen urban soils for geophysical anomalies, but also indicates that interpretation of these anomalies in terms of anthropogenic disturbances might not always be straightforward. This can be complicated further when metallic objects are prevalent in the studied urban environment. Specifically EMI is very sensitive to such local high conductors causing the geophysical signature of the soil material directly surrounding them to be compromised. Yet, the guaranteed detection of metallic objects may be an advantage in case they represent major targets in the site's investigation.[38] In any case, the detailed 3D soil information provided by the sensor combination offers a sound guide for the initial sampling design of invasive investigation. So-designed boring investigation can serve as ground truth and can aid in selecting the relevant geophysical anomalies for more in-depth investigation. Generally, we conclude that the proposed methodology is particularly valuable in an exploratory phase of urban soil assessment, to direct future (invasive) investigation and to support the intra- and extrapolation of information derived therefrom.

Acknowledgements

The authors would like to thank Gert Moerenhout and Sven Van Daele from the Soil Remediation Fund for Petrol Stations (BOFAS) for introducing this case study and for providing all the earlier collected site information. We also thank the owner-occupiers for their kind hospitality during our visits and Valentijn Van Parys for his help with the EMI and GPR surveys.

References

1 C. R. De Kimpe and J. L. Morel, *Soil Sci.*, 2000, **165**(1), 31-40.

2 A. Lehmann and K. Stahr, *J. Soils and Sediments*, 2007, **7**(4), 247-260.

3 H. Meuser, in *Contaminated Urban Soils.* Environmental pollution, 18. ed. B. J. Alloway and J. T. Trevors, Springer Science, New York, 2010, ch. 2, pp. 5-27 .

4 S. Norra and D. Stüben, *J. Soils and Sediments*, 2003, **3**(4), 230-233.

5 J. D. Redman, in *Ground Penetrating Radar: Theory and Applications* ed. H. M. Jol, Elsevier Science, Amsterdam, 2009, ch. 8, pp. 247-269.

6 V. I. Adamchuk, J. W. Hummel, M. T. Morgan and S. K. Upadhyaya, *Comput. Electron. Agric.*, 2004, **44**, 71-91.

7 D. L. Corwin and S. M. Lesch, *Comput. Electron. Agric.*, 2005, **46**, 11-43.

8 L. Verdonck, D. Simpson, W. M. Cornelis, A. Plyson, J. Bourgeois, R. Docter and M. Van Meirvenne, *Archaeological Prospection*, 2009, **16**, 193-202.

9 P. De Smedt, M. Van Meirvenne, D. Herremans, J. De Reu, T. Saey, E. Meerschman, P. Crombé, and W. De Clercq, *Sci. Rep.*, 2013, **3**(1517), 1-5.

10 T. Saey, M. Van Meirvenne, P. De Smedt, W. Neubauer, I. Trinks, G. Verhoeven, and S. Seren, *Eur. J. Soil Sci.*, 2013, **64**, 716-727.

11 J. M. Carcione, G. Seriani, and D. Gei, *J. Appl. Geophys.*, 2003, **52**(4), 177-191.

12 N. J. Cassidy, *J. Contam. Hydrol.*, 2007, **94**, 49-75.

13 M. L. Brewster, A. P. Annan, J. P. Greenhouse, B. H. Kueper, G. R. Olhoeft, J. D. Redman and K. A. Sander, *Ground Water*, 1995, **33**(6), 977-987.

14 J. J. Daniels, R. Roberts and M. Vendl, *J. Appl. Geophys.*, 1995, **33**(1-3), 195-207.

15 J. C. Santamarina and M. Fam, *J. Environ. Eng. Geophys.*, 1997, **2**, 37-52.

16 S. Jin, P. Fallgren, J. Cooper, J. Morris and M. Urynowicz, *J. Environ. Sci. Health, Part A: Toxic/Hazard. Subst. Environ. Eng.*, 2008, **43**(6), 584-588.

17 H. P. Martinelli, F. E. Robledo, A. M. Osella and M. de la Vega, *J. Appl. Geophys.*, 2012, **77**, 21-29.

18 E. A. Atekwana, W. A. Sauck and D. D. Werkema, *J. Appl. Geophys.*, 2000, **44**(2-3), 167-180.

19 E. D. Guy, J. J. Daniels, J. Holt and S. J. Radzevicius, *J. Environ. Eng. Geophys.*, 2000, **5**(2), 11-19.

20 M. de la Vega, A. Osella and E. Lascano, *J. Appl. Geophys.*, 2003, **54**, 97-109.

21 W. A. Sauck, *J. Appl. Geophys.*, 2000, **44**, 151-165.

22 D. D. Werkema Jr., E. A. Atekwana, A. L. Endres, W. A. Sauck and D. P. Cassidy, *Geophys. Res. Lett.*, 2003, **30**(12), 1647.

23 E. A. Atekwana and E. A. Atekwana, *Surv. Geophys.*, 2010, **31**, 247-283.

24 E. Auken, L. Pellerin, N. B. Christensen and K. Sørensen, *Geophys.*, 2006, **71**(5), G249-G260.

25 VLAREBO, Flemish Soil Remediation Decree ratified by the Flemish Government on 14 December 2007, Belgisch Staatsblad, April 22, 2008.

26 G. V. Keller and F. C. Frischknecht, *Electrical methods in geophysical prospecting*, Pergamon Press, Oxford, 1966.

27 J. D. McNeill, *Electromagnetic terrain conductivity measurements at low induction number, Technical Note TN-6,* Geonics Limited, Ontario, 1980.

28 T. Saey, D. Simpson, L. Cockx and M. Van Meirvenne, *Soil Sci. Soc. Am. J.*, 2009, **73**(1), 7-12.

29 D. Simpson, A. Lehouck, M. Van Meirvenne, J. Bourgeois, E. Thoen and J. Vervloet, *Geoarchaeol. Int. J.*, 2008, **23**(2), 305-319.

30 K. R. Sheets and J. M. Hendrickx, *Water Resour. Res.*, 1995, **31**(10), 2401-2409.

31 P. Goovaerts, *Geostatistics for Natural Resource Evaluation*, Oxford University Press, New York, USA, 1997.

32 T. Saey, M. Van Meirvenne, M. Dewilde, F. Wyffels, P. De Smedt, E. Meerschman, M. M. Islam, F. Meeuws and L. Cockx, *Near Surf. Geophys.*, 2011, **9**, 309-317.

33 S. Koppenjan, in *Ground Penetrating Radar: Theory and Applications,* ed. H. M. Jol, Elsevier Science, Amsterdam, 2009, ch. 3, pp. 73-97.

34 N. J. Cassidy, in *Ground Penetrating Radar: Theory and Applications*, ed. H. M. Jol, Elsevier Science, Amsterdam, 2009, ch. 5, pp. 141-176.

35 J. D. Rhoades and J. van Schilfgaarde, *Soil Sci. Soc. Am. J.*, 1976, **40**(5), 647-651.

36 ISO 11277, Soil quality - Determination of particle size distribution in mineral soil material - Method by sieving and sedimentation, 2009.

37 ISO/DIS 9377-4, Water Quality - Determination of hydrocarbon oil index - Part 4: Method using solvent extraction and gas chromatography, 1999.

38 E. Van De Vijver, M. Van Meirvenne, T. Saey, S. Delefortrie, P. De Smedt, J. De Pue and P. Seuntjens, *Eur. J. Soil Sci.*, 2015, DOI: 10.1111/ejss.12229.

39 T. Saey, M. Van Meirvenne, H. Vermeesch, N. Ameloot and L. Cockx, *Geoderma*, 2009, **150**, 389-395.

40 J. P. Boudreault, J. S. Dubé, M. Chouteau, T. Winiarski and É. Hardy, *Eng. Geol.*, 2010, **116**, 196-206.

41 D. Simpson, A. Lehouck, M. Van Meirvenne, J. Bourgeois, E. Thoen and J. Vervloet, *Geoarchaeol. Int. J.*, 2008, **23**(2), 305-319.

42 D. Simpson, M. Van Meirvenne, T. Saey, H. Vermeersch, J. Bourgeois, A. Lehouck, L. Cockx and U. W. A. Vitharana, *Archaeol. Prospect.*, 2009, **16**, 91-102.

43 F. André, C. van Leeuwen, S. Saussez, R. Van Durmen, P. Bogaert, D. Moghadas, L. de Rességuier, B. Delvaux, H. Vereecken and S. Lambot, *J. Appl. Geophys.*, 2012, **78**, 113-122.

44 M. M. Islam, E. Meerschman, T. Saey, P. De Smedt, E. Van De Vijver, S. Delefortrie and M. Van Meirvenne, *Soil Sci. Soc. Am. J.*, 2014, **78**, 579-588.

45 R. A. Omonode and T. J. Vyn, *Soil Sci.*, 2006, **171**(3), 223-238.

46 J. Kühn, A. Brenning, M. Wehrhan, S. Koszinski and M. Sommer, *Precision Agric.*, 2009, **10**(6), 490-507.

47 S. M. DeRyck, J. D. Redman and A. P. Annan, in *Proceedings of the symposium on the application of geophysics to engineering and environmental problems (SAGEEP),* Environmental and Engineering Geophysical Society, Wheat Ridge, CO, United States, 1993, pp. 5-19.

48 P. Fine, E. R. Graber and B. Yaron, *Soil Technol.*, 1997, **10**, 133-153.

49 M. Yang, Y. S. Yang, X. Du, Y. Cao and Y. Lei, *Water, Air, Soil Pollut.*, 2013, **224**(3), 1439.

50 D. Minai-Tehrani, P. Rohanifar and S. Azami, *Int. J. Environ. Sci. Technol.*, 2015, **12**, 1253-1260.

Figure captions

Fig. 1 Outline map of the study site with indication of the invasive investigation locations of the environmental assessment carried out between 2008 and 2012 and the consequent delineation of the soil contamination with petroleum hydrocarbons according to the TPH concentration thresholds provided by the Flemish soil remediation legislation (background value 50 mg/kg DM, target value 300 mg/kg DM and soil remediation threshold 750 mg/kg DM) (left); aerial photograph of the study site in 2012 which still shows stored vehicles at the parking area (right)

Fig. 2 a EC_a maps for the four coil configurations of the EMI sensor; measurement values outside the colour scale were assigned the same colour as the scale limits; **b** FEMP map; **c** 1HCP EC_a map with indication of anomalies A and B, and the locations selected for additional boring investigation of anomaly B

Fig. 3 Horizontal GPR slices mapping the signal magnitude at the indicated depths. The depth is expressed both in two-way travel time (left) and in meters (right); the conversion between these units is based on a RDP of 12.62 and a time zero of 2.83 ns. The greyscale contrast has been optimised for each slice separately. On the upper slice, transect EF is indicated, of which the vertical GPR profile is shown in Fig. 4

Fig. 4 Vertical GPR profile showing the real part of the GPR response in function of depth along transect EF, without (top) and with (bottom) indication of the contrasting interface

Fig. 5 a Schematic representation of the soil profiles at the six locations indicated in Fig. 2c showing four different soil layers in the upper 1.75 m of soil, with an illustration of the actual observation for 10-60 cm depth at location 3; **b** EC_p (top axis) in function of depth ("🗀"; the vertical lines indicate the depth intervals for which the measurements are representative) and the local GPR signal magnitude (bottom axis) in function of depth divided by the local maximum magnitude (relative); the depth is expressed both in meters (left axis) and in two-way travel time (right axis) **c** clay fraction (upper top axis, "🔔"), OM content (lower top axis, "➂") and TPH concentration (bottom axis, "✇") in function of depth; the vertical dashed line indicates the LOD (20 mg/kg DM) for the TPH concentration; TPH analysis results below the LOD are represented by a concentration of 10 mg/kg DM

Fig. 6 Field verification of the interpretation of anomaly A (Fig. 2c) as fill with demolition debris (left) and aerial photograph of the site taken in 1986 showing the former building and aboveground infrastructure near the location of anomaly A (Source: Department of Archaeology, Ghent University, J. Semey) (right)

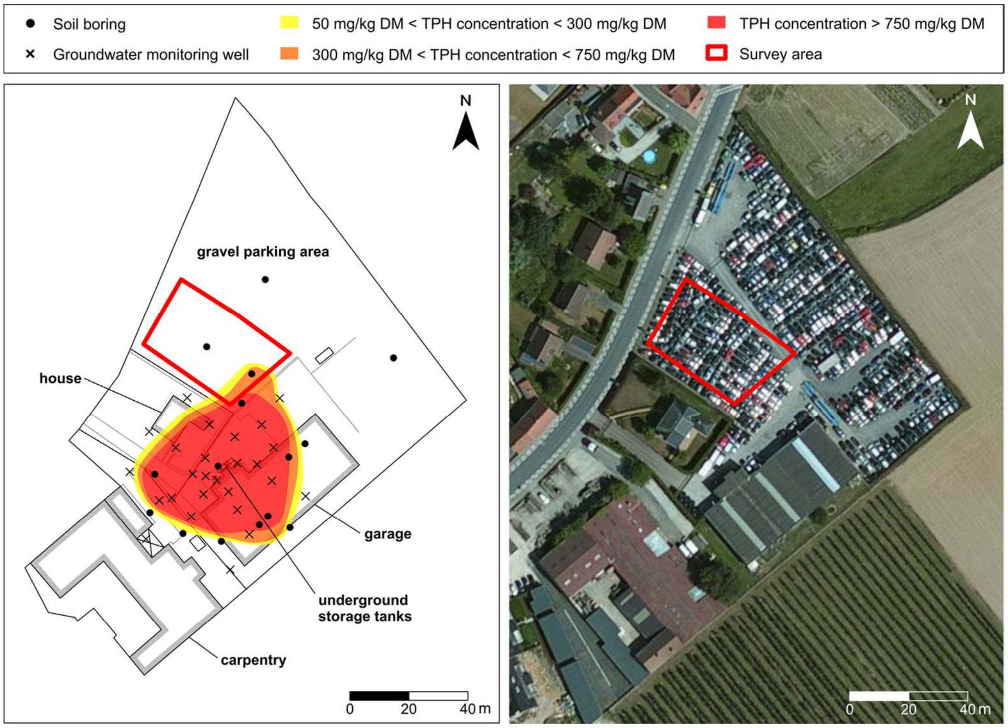

Fig. 1 Outline map of the study site with indication of the invasive investigation locations of the environmental assessment carried out between 2008 and 2012 and the consequent delineation of the soil contamination with petroleum hydrocarbons according to the TPH concentration thresholds provided by the Flemish soil remediation legislation (background value 50 mg/kg DM, target value 300 mg/kg DM and soil remediation threshold 750 mg/kg DM) (left); aerial photograph of the study site in 2012 which still shows stored vehicles at the parking area (right)
125x90mm (300 x 300 DPI)

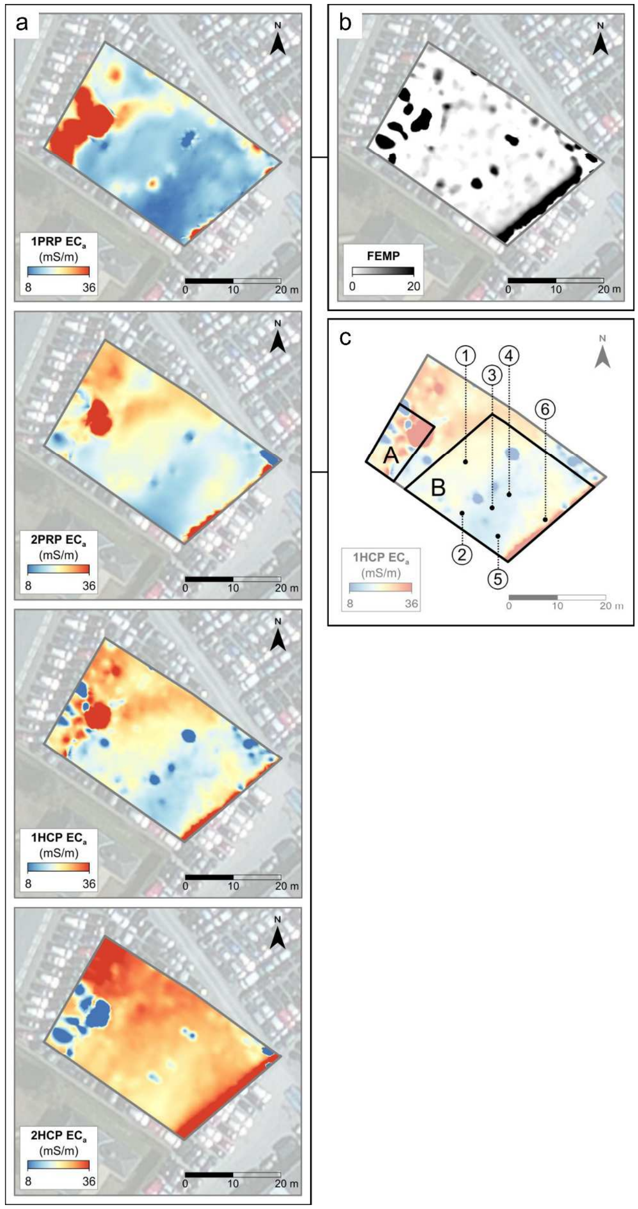

282x537mm (300 x 300 DPI)

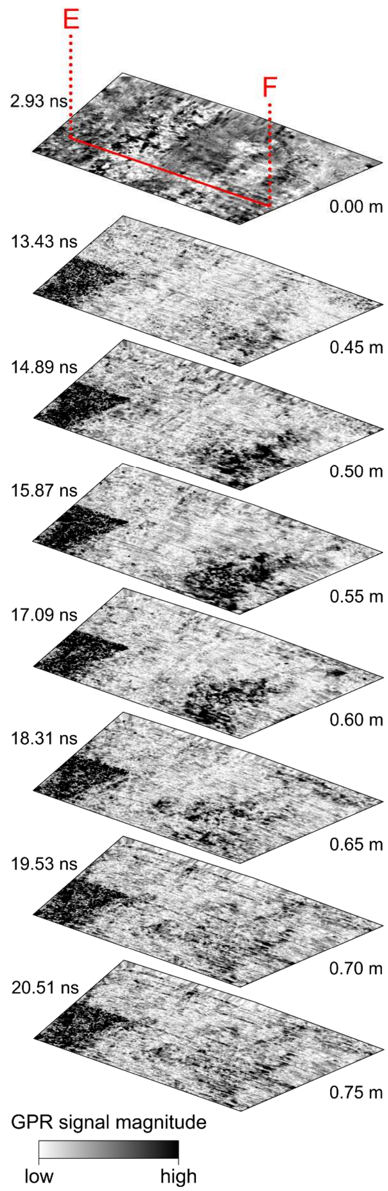

Fig. 3 Horizontal GPR slices mapping the signal magnitude at the indicated depths. The depth is expressed both in two-way travel time (left) and in meters (right); the conversion between these units is based on a RDP of 12.62 and a time zero of 2.83 ns. The greyscale contrast has been optimised for each slice separately. On the upper slice, transect EF is indicated, of which the vertical GPR profile is shown in Fig. 4

234x705mm (300 x 300 DPI)

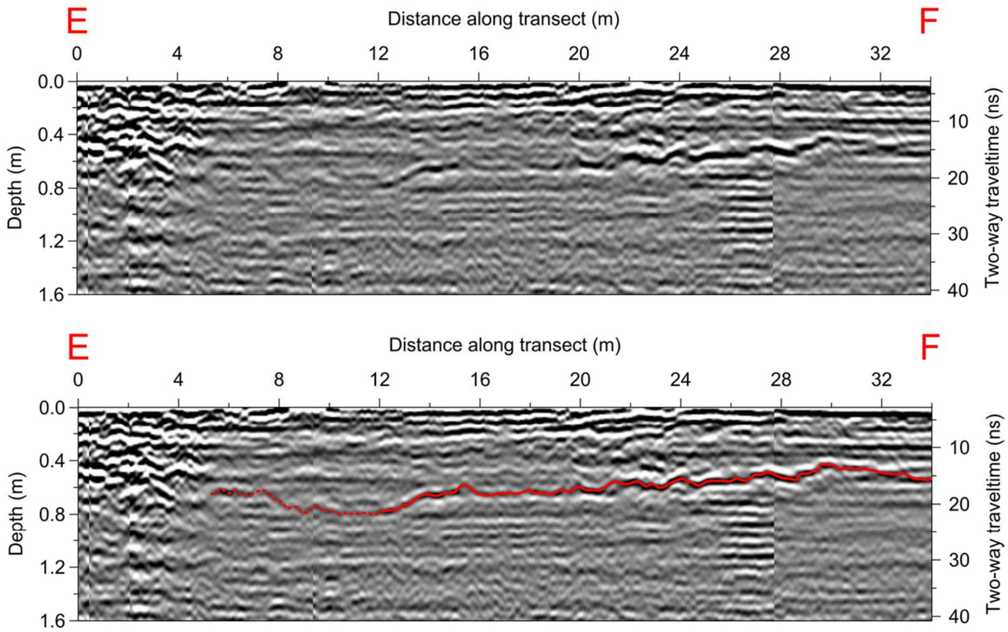

Fig. 4 Vertical GPR profile showing the real part of the GPR response in function of depth along transect EF, without (top) and with (bottom) indication of the contrasting interface
110x70mm (300 x 300 DPI)

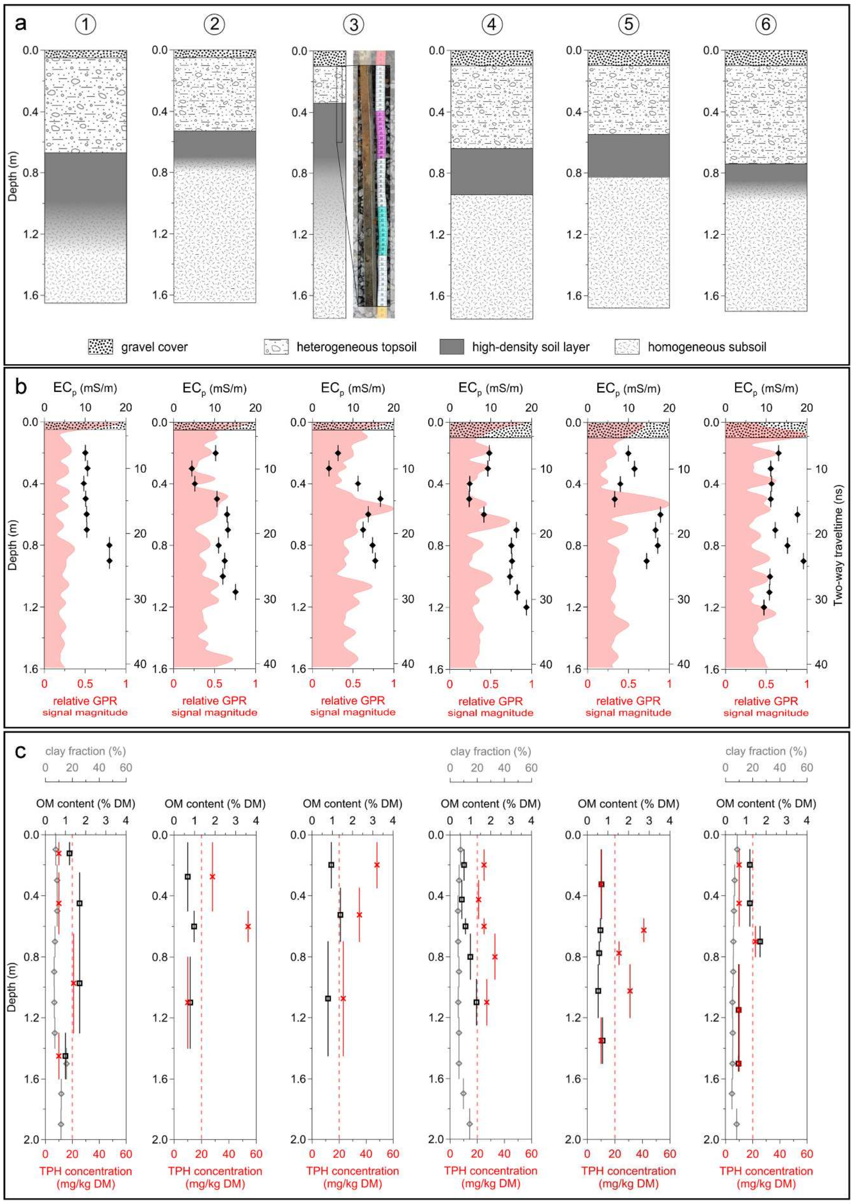

Fig. 5 a Schematic representation of the soil profiles at the six locations indicated in Fig. 2c showing four different soil layers in the upper 1.75 m of soil, with an illustration of the actual observation for 10-60 cm depth at location 3; b ECp (top axis) in function of depth ("0"; the vertical lines indicate the depth intervals for which the measurements are representative) and the local GPR signal magnitude (bottom axis) in function of depth divided by the local maximum magnitude (relative); the depth is expressed both in meters (left axis) and in two-way travel time (right axis) c clay fraction (upper top axis, "%"), OM content (lower top axis, ")") and TPH concentration (bottom axis, ">") in function of depth; the vertical dashed line indicates the LOD (20 mg/kg DM) for the TPH concentration; TPH analysis results below the LOD are represented by a concentration of 10 mg/kg DM

234x331mm (300 x 300 DPI)

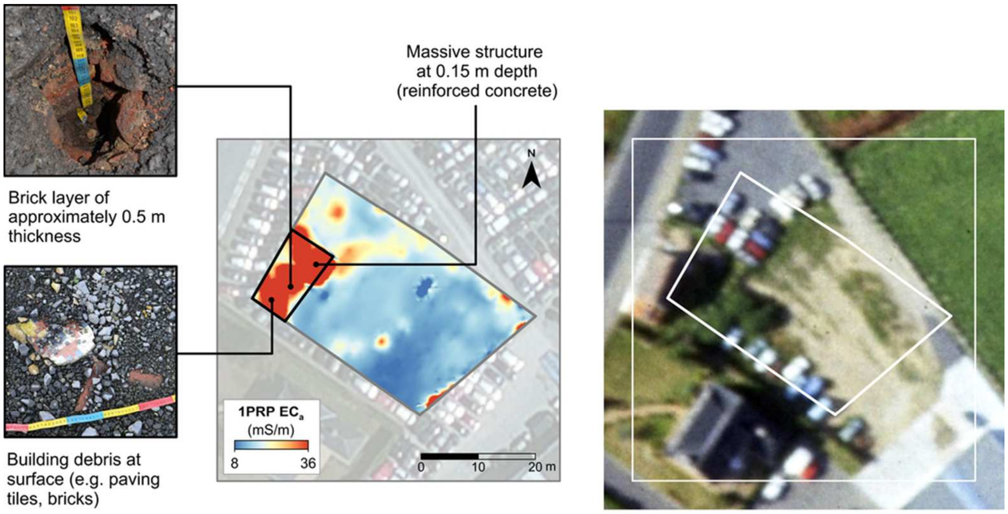

88x45mm (300 x 300 DPI)